Supporting Information

Galinato et al. 10.1073/pnas.1200345109

SI Materials and Methods

Expression and Purification of Isotope-Labeled *Hydrogenobacter thermophilus* cytochrome c_{552}. *Hydrogenobacter thermophilus* cytochrome c_{552} (*Ht* Cyt *c*) was expressed in *Escherichia coli* using the pSHC552 plasmid (Amp^r) (1). The appropriate *E. coli* strain (*vide infra*) was cotransformed with pSHC552 and pEC86 (Cm^r) (2); pEC86 contains genes *ccmA–ccmH* of the cytochrome *c* maturation system that facilitates heme attachment to the polypeptide (pp). To express $^{13}C_5{}^{15}N$-methionine (Met) *Ht* Cyt *c*, the protein was expressed in a Met auxotrophic strain of *E. coli*, B834. Competent B834 cells were purchased from Novagen. All other samples were expressed in BL21 (DE3) (Invitrogen).

All growths were performed in modified minimal medium (3). $FeSO_4{\cdot}7\,H_2O$ (500 mg/L) was replaced with $^{57}FeSO_4{\cdot}1.2\,H_2O$ (20 mg/L). ^{57}Fe metal was reacted with 40% (vol/vol) aqueous H_2SO_4 to produce a white solid, which was filtered to obtain $^{57}FeSO_4{\cdot}1.2\,H_2O$. To express protein with isotopically labeled pp ($^{13}C^{15}N$-pp *Ht* Cyt *c*), D-glucose (5 g) and NH_4Cl (1 g) were replaced with $^{13}C_6$-D-glucose (3 g) and $^{15}NH_4Cl$ (1 g), respectively. The heme remained unenriched because the medium was supplemented with a metabolic precursor to heme [16.8 mg/L 5-aminolevulinic acid (ALA)] at natural isotopic abundance. To express $^{13}C_5{}^{15}N$-Met-*Ht* Cyt *c*, the medium was supplemented with 100 mg/L $^{13}C_5{}^{15}N$-Met. To express $^{13}C_8$-heme–labeled *Ht* Cyt *c* (Fig. S2), 16.8 mg/L ALA was replaced with 16.8 mg/L 4-^{13}C-ALA (4). Isotopes were purchased from Cambridge Isotope Laboratories.

Cells from overnight growths (~16 h, 10 mL) in LB medium were centrifuged at 4,000 × g and resuspended in 5 mL of minimal medium before inoculation. Cells were grown in 1 L of minimal medium supplemented with 50 μg/mL ampicillin and chloramphenicol in 4-L flasks for 24 h at 37 °C with a shaking speed of 120 rpm. The cells were harvested by centrifugation and frozen at −20 °C. Purification was performed as previously described (1). Purified protein was exchanged into 10 mM ammonium acetate buffer and lyophilized.

Nuclear Resonance Vibrational Spectroscopy. Immediately before data collection, lyophilized, ^{57}Fe-labeled *Ht* Cyt *c* was dissolved in 50 mM Hepes buffer containing 10% (vol/vol) glycerol (pH 7.0, 16.5–18 mM protein). K_2IrCl_6 was added to a concentration of 25 mM to prevent sample reduction. The protein samples (70 μL) were loaded into 3.5-mm × 2-mm × 16-mm acrylic nuclear resonance vibrational spectroscopy (NRVS) cells and frozen in liquid N_2. NRVS data were collected at beam line 3-ID-XOR of the Advanced Photon Source at Argonne National Laboratory. A description of the parameters used for sample excitation and probing of the scattered light is provided by Lehnert et al. (5). The samples were maintained at cryogenic temperatures using a liquid helium cryocooler during the accumulation of NRVS data. The NRVS spectra were recorded between −50 and 65 meV in steps of 0.25 meV. Each scan took ~40 min, and all scans were normalized to the intensity of the incident beam and added. The NRVS raw data were converted to the vibrational density of states (VDOS) using the program Phoenix, an in-house program at APS written by Wolfgang Sturhahn (6). An excellent discussion on the conversion of raw intensity to VDOS is presented by Sage et al. (6), Leu et al. (7), and Lehnert et al. (8).

Density Functional Theory Calculations. The high-resolution crystal structure of *Ht* Cyt *c* [Protein Data Bank (PDB) ID code 1YNR] was used as a starting point for building an active-site model for the density functional theory (DFT) calculations. The active-site model used here consists of heme *c* covalently linked to the pp through two thioether bonds in a Cys12-Met13-Ala14-Cys15-His16 (CMACH) motif; the Met61 axial ligand to iron, where the Met was simplified by truncating the carboxyl and amino groups; and a formaldehyde molecule in place of Pro, which forms a hydrogen bond to the His16 HNδ^{π} proton. Hydrogens were added to the active-site model through the "View–Hydrogens" option in GaussView 5.0 (Gaussian, Inc.). The CMACH linkage was simplified by truncating the side chains of Met13 and Ala14 and replacing them with hydrogen atoms. Importantly, the optimized structure shows that the heme axial Met dihedral angle (the dihedral angle between the N_{His}-Fe-S_{Met}-C_γ atoms) differs from the crystal structure by 23°. Deviations in the geometry along the CMACH motif are also observed. For example, the C_{Met}-C_γ-S_{Cys} angle of Cys12 in the model complex is 16° larger than that in the crystal structure. A total of 142 atoms represent the coordinates of this active site model of *Ht* Cyt *c*. All atoms were optimized using the BP86 functional (9, 10) and the LanL2DZ* basis set (5, 11–13) as implemented in Gaussian 03 (Gaussian, Inc.). Vibrational frequencies were calculated for the optimized structure using the same functional and basis set.

Quantum Chemistry-Centered Normal Coordinate Analysis. To simulate the NRVS spectrum, the quantum chemistry-centered normal coordinate analysis (QCC-NCA) package was used. A description of the program's utilities is nicely summarized by Lehnert et al. (8). To describe the system, 519 internal coordinates and 134,940 (diagonal and off-diagonal) force constants were required. Of these, 160 adjustable parameters were used for the QCC-NCA simulation (Table S1), but changes from the calculated values of these force constants were kept to a minimum in the simulation. Manual adjustments were made on the porphyrin core diagonal force constants to reproduce the vibrational frequencies, isotope shifts, and NRVS VDOS intensities of the experimental data. The experimental spectra of the $^{13}C^{15}N$-pp–, $^{13}C_5{}^{15}N$-Met–, and $^{13}C_8$-heme–labeled ferric proteins were also used as a guide in the manipulation of the force constants to fit the DFT-obtained NRVS spectrum to the experimental data properly. A list of the force constants included in the NCA simulation is presented in Table S1.

In addition to simulating the experimental NRVS data of *Ht* Cyt *c*, the effect of the position and stereochemistry of the distal Met on the intensities and energies of the NRVS vibrational features was also studied. This was done by manually changing the dihedral angles and the stereochemistry of Met, followed by recalculation of the NRVS spectra. It is noted that a 23° change in the dihedral angle of the distal Met is observed in the optimized structure of the model relative to the crystal structure. However, as shown in Fig. 4 (*Upper Left*), adjusting the position of Met to the crystallographically observed dihedral angle has only marginal effects on the simulated NRVS spectrum.

1. Karan EF, Russell BS, Bren KL (2002) Characterization of *Hydrogenobacter thermophilus* cytochromes c(552) expressed in the cytoplasm and periplasm of Escherichia coli. *J Biol Inorg Chem* 7:260–272.
2. Fee JA, et al. (2000) Integrity of thermus thermophilus cytochrome c552 synthesized by Escherichia coli cells expressing the host-specific cytochrome c maturation genes, ccmABCDEFGH: Biochemical, spectral, and structural characterization of the recombinant protein. *Protein Sci* 9:2074–2084.
3. Liptak MD, Wen X, Bren KL (2010) NMR and DFT investigation of heme ruffling: Functional implications for cytochrome *c*. *J Am Chem Soc* 132:9753–9763.
4. Rivera M, Walker FA (1995) Biosynthetic preparation of isotopically labeled heme. *Anal Biochem* 230:295–302.
5. Lehnert N, et al. (2010) Nuclear resonance vibrational spectroscopy applied to [Fe(OEP)(NO)]: The vibrational assignments of five-coordinate ferrous heme-nitrosyls and implications for electronic structure. *Inorg Chem* 49:4133–4148.

6. Sage JT, et al. (2001) Nuclear resonance vibrational spectroscopy of a protein active-site mimic. *J Phys Condens Matter* 13:7707–7722.
7. Leu BM, et al. (2009) Vibrational dynamics of iron in cytochrome C. *J Phys Chem B* 113: 2193–2200.
8. Lehnert N, et al. (2010) Oriented single-crystal nuclear resonance vibrational spectroscopy of [Fe(TPP)(MI)(NO)]: Quantitative assessment of the *trans* effect of NO. *Inorg Chem* 49:7197–7215.
9. Becke AD (1988) Density-functional exchange-energy approximation with correct asymptotic behavior. *Phys Rev A* 38:3098–3100.
10. Perdew JP (1986) Density-functional approximation for the correlation energy of the inhomogeneous electron gas. *Phys Rev B Condens Matter* 33:8822–8824.
11. Wadt WR, Hay PJ (1985) Ab initio effective core potentials for molecular calculations. Potentials for the transition metal atoms Sc to Hg. *J Chem Phys* 82:270–283.
12. Wadt WR, Hay PJ (1985) Ab initio effective core potentials for molecular calculations. Potentials for main group elements Na to Bi. *J Chem Phys* 82:284–298.
13. Wadt WR, Hay PJ (1985) Ab initio effective core potentials for molecular calculations. Potentials for K to Au including the outermost core orbitals. *J Chem Phys* 82:299–311.

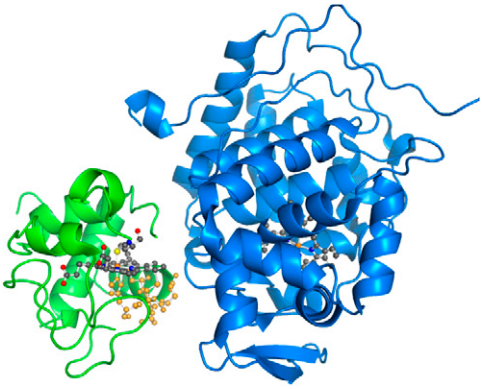

Fig. S1. Cytochrome *c* peroxidase (blue)/Cyt *c* (green) complex from *Saccharomyces cerevisiae* [Protein Data Bank (PDB) ID code 2PCB]. The active sites of the proteins are shown as ball-and-stick representations. The Cys-X-X-Cys-His residues in Cyt *c* are highlighted in orange.

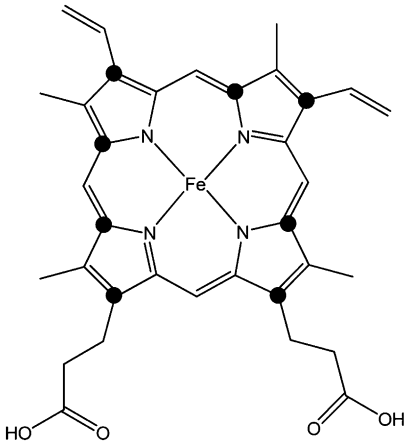

Fig. S2. Labeling scheme of the porphyrin for $^{13}C_8$-heme–labeled *Ht* Cyt *c* prepared using 4-^{13}C-ALA as a heme precursor.

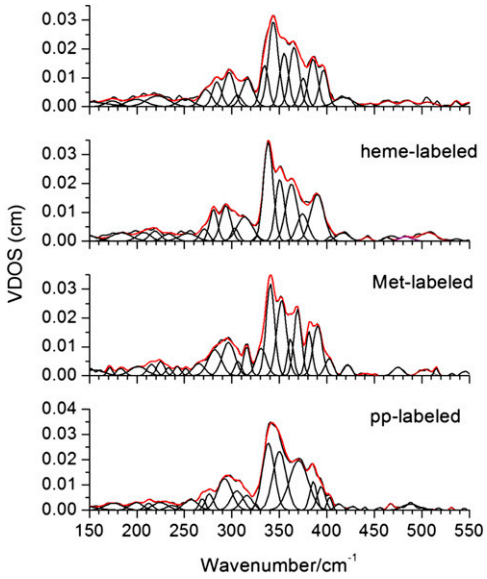

Fig. S3. NRVS spectra of ferric *Ht* Cyt *c* and of corresponding $^{13}C_8$-heme–, $^{13}C^{15}N$-Met–, and $^{13}C^{15}N$-pp–labeled proteins. Gaussian fits of these data are included.

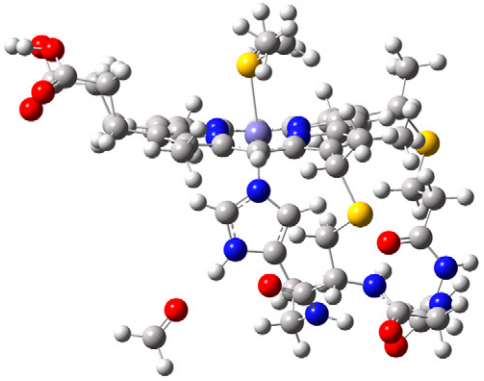

Fig. S4. Optimized structure of the active site model of ferric *Ht* Cyt *c* [Protein Data Bank (PDB) ID code 1YNR] shows the Cys12-Met13-Ala14-Cys15-His16 pentapeptide on the proximal side of the heme and Met61 on the distal side. The yellow, purple, red, blue, and gray spheres represent sulfur, heme iron, oxygen, nitrogen, and carbon, respectively.

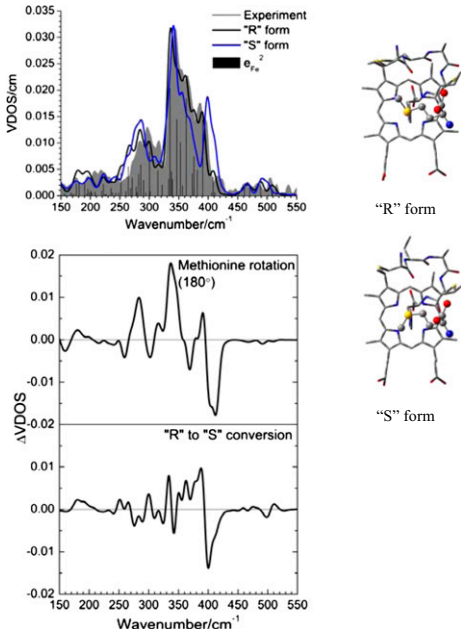

Fig. S5. (*Upper*) Simulated NRVS spectra of ferric *Ht* Cyt *c* as a function of Met stereochemistry ("R" and "S" forms). The experimental NRVS spectrum is shaded in gray. The vertical ticks correspond to Fe motions of each mode and their contributions to the total spectrum. (*Lower*) Difference spectra obtained by subtracting the simulated spectrum of the 180° rotated Met ferric *Ht* Cyt *c* from that of the "normal" form (*Top*) and that generated by subtracting the spectrum of the S Met form from that of the R Met form (*Bottom*) are shown.

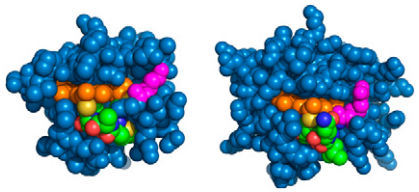

Fig. S6. Space-filling models of *Ht* Cyt *c* (*Left*) and *Saccharomyces cerevisiae* Cyt *c* (*Right*) (PDB: 1YCC) showing the positions of the Cys-X-X-Cys-His (CXXCH) residues and the solvent-exposed heme edge at pyrrole II. The CXXCH residues are shown in green, red, dark blue, and yellow (for carbon, oxygen, nitrogen, and sulfur); the basic residue at position 11 (*Ht*) and position 13 (yeast) is shown in magenta; the heme is shown in orange; and the rest of the pp is shown in blue.

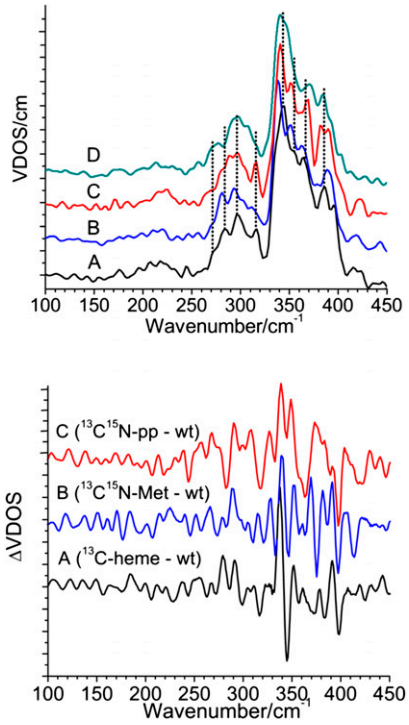

Fig. S7. (*Upper*) NRVS spectra of ^{57}Fe(III) *Ht* Cyt *c* (*A*) and $^{13}C_8$-heme–labeled (*B*), $^{13}C^{15}N$-Met–labeled (*C*), and $^{13}C^{15}N$-pp–labeled (*D*) protein. (*Lower*) Difference in NRVS spectra between ^{57}Fe(III) *Ht* Cyt *c* and $^{13}C_8$-heme–labeled (*A*), $^{13}C^{15}N$-Met–labeled (*B*), and $^{13}C^{15}N$-pp–labeled (*C*) protein. All protein samples were dissolved in 50 mM Hepes buffer containing 10% glycerol (pH 7.0, 16.5–18 mM). K_2IrCl_6 was added to a concentration of 25 mM to prevent sample reduction. wt, wild type.

Table S1. Complete list of force constants of ferric *Ht* Cyt *c* invoked in the fit of the NRVS data, based on the BP86/LanL2DZ* result

Force constant	BP86/LanL2DZ*	QCC-NCA
Fe-S_{Met} [1]	0.8004	0.9304
Fe-N_{His} [17]	1.4793	1.2393
Fe-N_{Pyr} [13–16]	1.6041, 1.6471, 1.6831, 1.7658	1.7341, 1.7371, 1.7531, 1.8158
[13]/[15], [14]/[16]	0.2702, 0.2068	0.2602, 0.2168
[1]/[17]	0.1368	0.1068
ν(pp)	4.9754, 6.3916, 3.8215, 4.8548, 6.6429, 3.8030, 4.9051, 6.1322, 3.9163, 3.7993, 2.8974, 2.4038, 2.7790, 2.3752	5.0754, 6.5916, 4.0215, 4.9548, 6.7429, 3.9030, 5.0051, 6.2322, 4.1163, 3.8993, 3.0974, 2.6038, 2.9990, 2.5852
ν(His)	4.5030, 3.5848, 5.4200, 6.7263	4.8030, 3.7948, 5.6300, 6.9363
N_{Pyr}-Fe-N_{Pyr} [189–192]	0.6687, 0.7264, 0.6418, 0.7258	0.7187, 0.7564, 0.7618, 0.7658
N_{His}-Fe-N_{Pyr} [185–188]	0.6322, 0.7433, 0.7330, 0.8545	0.7522, 0.8133, 0.8030, 0.9345
[17]/[182–184]	−0.0032, 0.1239, 0.1618	0.0132, 0.1039, 0.1118
[1]/[181]	−0.1057	−0.0857
S_{Met}-Fe-N_{Pyr} [181–184]	0.8228, 0.9602, 0.7333, 0.8575	0.8228, 0.9602, 0.7333, 0.8775
[1]/[185–186]	0.0049, 0.0152	0.0591, 0.0253
δ(pp)	0.9097, 1.2867, 0.5031	0.9697, 1.3267, 0.6931
δ(His) [366, 373, 386, 392]	0.8974, 0.5902, 0.7335, 0.8885	0.8174, 0.6402, 0.8135, 0.9685
δ(Met) [176]	1.1753	1.0553
[1]/[176]	−0.0603	−0.1028
[17]/[366–367]	0.1448, −0.0191	0.1948, −0.0461
Fe-S_{Met}-C [160–161]	1.1267, 1.1388	1.1667, 1.1788
δ_{ip}(porphyrin): pyrrole	2.4745, 2.6721, 2.5486, 2.3345, 2.4667, 2.5191, 2.5552, 2.4595	2.5045, 2.7021, 2.5786, 2.3645, 2.4967, 2.5491, 2.5852, 2.4895
δ_{ip}(porphyrin): methine	0.9723, 0.9810, 0.9480, 0.9907, 0.8326, 0.9892, 1.0825, 1.1071	0.8723, 0.8810, 0.8480, 0.8907, 0.8906, 1.0192, 1.2825, 1.2871
δ_{oop}(porphyrin): pyrrole	0.3094, 0.2744, 0.2569, 0.2588, 0.4453, 0.4371, 0.4401, 0.4239, 0.4874, 0.4738, 0.4278, 0.4182	0.2194, 0.1944, 0.1970, 0.1988, 0.4353, 0.4171, 0.4101, 0.4239, 0.4574, 0.4338, 0.4178, 0.3982
δ_{oop}(porphyrin): methine	0.3964, 0.3479, 0.3971, 0.3665, 0.3495, 0.3739, 0.3441, 0.3543	0.4264, 0.3779, 0.4271, 0.3965, 0.3796, 0.4039, 0.3741, 0.3843
δ(propionate)	0.8388, 1.2876, 0.6608, 0.6628	0.9588, 0.6876, 0.7607, 0.7628
τ(Met) [454–456]	0.1002, 0.1176, 0.2308	0.0901, 0.1276, 0.3708
τ(Fe-S_{Met}), τ(Fe-N_{His}) [453, 457]	0.2671, 0.7394	0.3401, 0.7894
[453]/[455, 457]	0.0127, 0.0670	0.0157, 0.0570
[1]/[455–454]	−0.0237, 0.0008, −0.0841	−0.0277, −0.008, −0.0941
τ(His)	0.1958, 0.9162, 1.4041, 1.1328, 0.2142, 3.05927, 1.1926	0.1558, 0.8562, 1.3541, 1.0728, 0.1642, 3.0552, 1.2026
τ(pp)	0.6040, 0.2829, 0.4318, 0.4898, 0.1951, 0.2157, 0.3853, 0.1713, 0.2249, 0.2368, 0.2427	0.6544, 0.3329, 0.4818, 0.4998, 0.2451, 0.2757, 0.4453, 0.2313, 0.2849, 0.2968, 0.3027
τ(porphyrin)	0.3289, 0.0587, 0.3573, 0.0461, 0.0276, 0.5344, 0.3043, 0.0289, 0.3066, 0.2514, 0.2653, 0.2318, 0.2636, 0.2777, 0.2437, 0.2626, 0.2479, 0.2187, 0.2577, 0.2009, 0.2828, 0.2522, 0.2210, 0.2976, 0.2035, 0.2535, 0.2206, 0.2299	0.3089, 0.0557, 0.3372, 0.0421, 0.0226, 0.5144, 0.2743, 0.0229, 0.3216, 0.2664, 0.2804, 0.2468, 0.2786, 0.2927, 0.2587, 0.2776, 0.2630, 0.2327, 0.2728, 0.2159, 0.2978, 0.2672, 0.2360, 0.3126, 0.2185, 0.2685, 0.2356, 0.2450
τ(proprionate)	0.7131, 0.7666, 0.2358, 0.0796	0.7331, 0.7866, 0.3458, 0.2296
$O_{Proline}$-H_{His} (H-bond)	0.3726	0.4026

δ_{ip}, in-plane bending mode; δ_{oop}, out-of-plane bending mode. The numbers in square brackets refer to the numbers designated for the corresponding internal coordinates in the force field. These are provided to unambiguously identify the given internal coordinates. The []/[] terms are nondiagonal elements.

Table S2. Condensed vibrational assignments for ferric *Ht* Cyt *c* based on the QCC-NCA simulation of the NRVS data

	QCC-NCA[†]			
Experiment, ν[cm^{-1}](Δ)*	ν[cm^{-1}]	sym/int[‡]	Polarization	Assignment
	147	/vw	ip/oop = 1.6:1	τ(His + pp)/ $\tau(CH_3)_{PyrII}$
	160	/vw	ip	τ(pp + His)/ τ(methyl)/ δ(pp)
	167	/vw	ip/oop = 0.75:1	τ(Met)/ ν(Fe-S_{Met})
	173	/vw	ip/oop = 1:1	δ(Fe-S_{Met}-C)/ τ(Met + Prop)/ δ(Met)
222	190	B_{1u}/vw	ip/oop = 1:1	γ_{13}/ τ(Prop)/ δ(Fe-S_{Met}-C)
	203	/vw	ip/oop = 1.25:1	Pyr. trans/ τ(Prop)
	224	/vw	ip	τ(Met)/ δ(Fe-S_{Met}-C)/ δ(Met)
273 (−2/−8/−4)	252	/w	ip/oop = 1:2	Pyr. swiv/ τ(Met)/ ν(Fe-N_{Pyr})
284 (−3/−1/−7)	264	/mw	ip/oop = 1.1:3	τ(pp)/ δ(pp)/ $\delta(C_\beta\text{-}C)_{sym}$
	278	/w	ip/oop = 1:1	τ(pp + Met)/ δ(Fe-S_{Met}-C)/ ν(Fe-S_{Met})/ $\delta(C_\beta\text{-}C)_{sym}$
297 (−4/−1/−5)	300	A_{2u}/m	oop	γ_7/ ν(Fe-S_{Met})/ ν(Fe-N_{His})/ $\delta(C_\beta\text{-}C)_{sym}$
306 (−3/0/na)	290	/w	ip/oop = 0.85:1	$\delta(C_\beta\text{-}C)_{sym}$/ His. rot/ Pyr. swiv
316 (−2/0/−8)	286	/mw	ip/oop = 1:4	τ(pp)/ δ(pp)/ $\gamma(C_\alpha\text{-}C_m)$
334 (−8/−3/−6)	315	/w	ip/oop = 2.7:1	$\delta(C_\beta\text{-}C)_{sym}$/ ν(Fe-N_{Pyr})
344 (−6/−4/−5)	335	E_u/vs	ip	ν_{50}
355 (−4/−3/−5)	347	E_u/vs	ip	ν_{50}/ Pyr. tilt
366 (−2/+3/+5)	363	A_{2u}/s	ip/oop = 1:9	γ_6
375 (−1/na/na)	376	/m	ip/oop = 1:4	Pyr. swiv/ τ(His)/ His. rot
385 (+6/−4/−1)	391	/s	ip/oop = 11:1	ν(Fe-N_{Pyr})/ His. rot/ Pyr. tilt/ τ(His)
397 (na/−7/−3)	381	/m	ip	Pyr. tilt/ Pyr. swiv
418 (0/+4/−15)	408	/w	ip	$\delta(C_\beta\text{-}C_a\text{-}C_b)_{PyrII}$/ ν(Fe-N_{Pyr})/ Pyr. tilt
464	471	/w	ip	Pyr. rot
485	489	/w	ip	Pyr. rot

Classifications of heme vibrations are taken from the study by Li et al. (1) [see also the study by Paulat et al. (2)]. His, histidine; ip, in-plane; na, not available; oop, out-of-plane; Prop, propionate groups; Pyr., pyrrole; ν, stretch; δ, bend; τ, torsion; γ, oop wag; γ_{13}, oop swivel (B_{1u}); γ_7, oop meso carbon wag; γ_6, oop pyrrole tilting (A_{2u}); ν_{50}, ν(Fe-N_{Pyr}) (E_u).

*(Δ) = ^{13}C, $^{13}C^{15}N$, and $^{13}C^{15}N$ isotope shifts in the heme-labeled, Met-labeled, and pp-labeled samples.

[†]Based on the BP86/LanL2DZ* calculation.

[‡]Symmetry (sym, in D_{4h}) and calculated intensity (int): m, medium, mw, medium weak; s, strong; vs, very strong; w, weak; vw, very weak.

1. Li X-Y, Czernuszewicz RS, Kincaid JR, Spiro TG (1989) Consistent porphyrin force field. 3. Out-of-plane modes in the resonance Raman spectra of planar and ruffled nickel octaethylporphyrin. *J Am Chem Soc* 111:7012–7023.
2. Paulat F, Praneeth VKK, Näther C, Lehnert N (2006) Quantum chemistry-based analysis of the vibrational spectra of five-coordinate metalloporphyrins [M(TPP)Cl]. *Inorg Chem* 45: 2835–2856.